Journal of Atmospheric and Solar-Terrestrial Physics 71 (2009) 470–476

Contents lists available at ScienceDirect

Journal of
Atmospheric and Solar-Terrestrial Physics

journal homepage: www.elsevier.com/locate/jastp

Observations of polar mesospheric summer echoes using PFISR during the summer of 2007

Roger H. Varney [a,*], Michael J. Nicolls [b], Craig J. Heinselman [b], Michael C. Kelley [a]

[a] School of Electrical and Computer Engineering, Cornell University, 320 Rhodes Hall, Ithaca, NY 14853, USA
[b] Center for Geospace Studies, SRI International, 333 Ravenswood Ave., Menlo Park, CA, USA

ARTICLE INFO

Article history:
Accepted 7 January 2009
Available online 20 January 2009

Keywords:
Polar mesospheric summer echoes (PMSE)
Poker Flat Incoherent Scatter Radar (PFISR)
Ionospheric irregularities

ABSTRACT

The Poker Flat Incoherent Scatter Radar (PFISR) has been running nearly continuously throughout the summer of 2007, which permits an unprecedented, long-term study of polar mesospheric summer echoes (PMSE) at UHF. When not being used for other operations, PFISR runs in its International Polar Year (IPY) mode. 176 examples of PMSE have been identified in the IPY dataset during the summer of 2007 on 42 different days. IPY data were examined from March through mid-September. The first event was observed on May 27, and the last on August 10. During the four months from May 14 through September 14 the IPY mode was run 57% of the time and PMSE was detected 3.3% of the time the mode was running. Thirty-eight percent of the days with data during these four months had at least one PMSE event. Seventy-three percent of the events occurred during the daytime, and of the 48 events at night, 31 were accompanied by auroral precipitation. The events that did not occur with aurora show a strong correlation with solar zenith angle, which suggests a dependence on background ionization. Events were observed in range gates centered at 81.2 and 85.5 km, with 141 of the 176 events in the lower gate. The events have a mean duration of 19.6 min, but events lasting as long as 106 min have been observed. The events have a mean reflectivity of 1.3×10^{-17} m^{-1}, which is a lower bound due to the possibility that the beam is not filled. A Lorentzian power spectrum was assumed to fit for the half-power half-width (HPHW) of the measured autocorrelation functions. The HPHWs which could be measured have a mean of 14.8 m/s, with a standard deviation of 11.1 m/s.

1. Introduction

Polar mesospheric summer echoes (PMSE) are strong, coherent radar echoes originating in the cold polar summer mesopause region. Echoes which were later understood to be PMSE were first observed in the late 1970s and early 1980s at VHF near 50 MHz (Czechowsky et al., 1979; Ecklund and Balsley, 1981). Since then, PMSE has also been observed at higher frequencies, including the 224 MHz EISCAT VHF (Röttger et al., 1988), the 500 MHz EISCAT Svalbard Radar (Hall and Röttger, 2001), the 933 MHz EISCAT UHF (Röttger et al., 1990; La Hoz et al., 2006; Rapp et al., 2008), the 1.29 GHz Sondrestrom Radar (Cho et al., 1992b), and the 450 MHz Poker Flat Advanced Modular Incoherent Scatter Radar (PFISR) (Nicolls et al., 2007, 2008).

PMSE is thought to be associated with the presence of charged ice particles known to exist in the polar mesosphere. These ice particles reduce the dissipation rate of electron density fluctuations, an idea first put forward by Kelley et al. (1987) and refined by Cho et al. (1992a). Recent developments by Rapp and Lübken (2003) have shown that the frequency dependence of PMSE observations can be explained by this theory (see also the review by Rapp and Lübken, 2004). In addition, Rapp and Lübken (2003) showed that the diffusion times of the density fluctuations are large enough to decouple the existence of PMSE from the actual neutral turbulence. This so-called fossil turbulence explains why PMSE and neutral air turbulence are often not observed to occur in the same volumes by ground and in situ instrumentation (e.g., Lübken et al., 2002).

While there have been many observations of PMSE at VHF, there are few systems with sufficient sensitivity to observe the echoes at higher frequencies. In this paper, we utilize the unattended observational capabilities of the ~450 MHz Poker Flat Incoherent Scatter Radar (PFISR) to study the statistics of PMSE occurrence at UHF. The PFISR "background" mode operates whenever the radar is not scheduled for user experiments. While not designed for PMSE studies, the mode allows for PMSE detection and the extraction of some spectral information. Observations of PMSE at small Bragg wavelengths (i.e., at UHF) may be particularly unique because of their potential to probe the energy dissipation region of turbulence. Numerical simulations of turbulence and their associated radar backscatter quantities (e.g., Fritts et al., 2003; Gibson-Wilde et al., 2000) have shown that VHF

* Corresponding author.
E-mail address: rhv5@cornell.edu (R.H. Varney).

1364-6826/$ - see front matter © 2009 Elsevier Ltd. All rights reserved.
doi:10.1016/j.jastp.2009.01.002

echoes may be most indicative of regions where the thermal dissipation rate is largest, i.e., at the edges of turbulent structures. UHF backscatter, on the other hand, may be more sensitive to the region where the energy dissipation maximizes, which is the center of the turbulent volume. Thus, measurements at different scales are complementary in the sense that they may be probing different aspects/regions of the associated turbulence.

2. Experiment and methodology

PFISR is located in the interior of Alaska near Fairbanks at 65.13°N, 147.47°W. The International Polar Year (IPY) mode is a low duty cycle (~1%), "background" mode that includes an alternating code transmission at 449.0 MHz. A single beam is utilized which is pointed up the local magnetic field line (Az: −154.3°, El: 77.5°). A 480 μs, 16-baud pulse encoded with a strong, randomized alternating code (Lehtinen and Häggström, 1987) is transmitted alongside a single 30 μs uncoded pulse, typically used for zero-lag normalization. The zeroth lag of the alternating code has poor range ambiguity, but the other properly decoded 15 lags have 4.5 km range resolution. Accounting for the elevation angle of the beam, the corresponding altitude resolution is $4.5\sin(77.5^\circ) = 4.39$ km. Online integration consists of summing 160 pulses over 16 s intervals to produce estimates of the autocorrelation function (ACF). Noise samples are also taken, and an injected calibration pulse at 364 K is used for absolute calibration of the received power.

This experiment was not specifically designed for PMSE and consequently does not have adequate range resolution or spectral resolution to resolve the echoes. However, PMSE can be identified, providing statistical information useful given that this mode operated ~57% of the available operating time of the system during the period from May 14 until September 14. All local times were covered roughly evenly. This data coverage is illustrated in Fig. 1.

3. Observations

Plots of the signal-to-noise ratio (SNR) were visually searched for long-lived, strong echoes that were confined in altitude to one or two range gates for all the data between March and late September. PMSE events were only observed between late May and early August. An automated algorithm which searched for narrow layers was used to identify PMSE events between late May

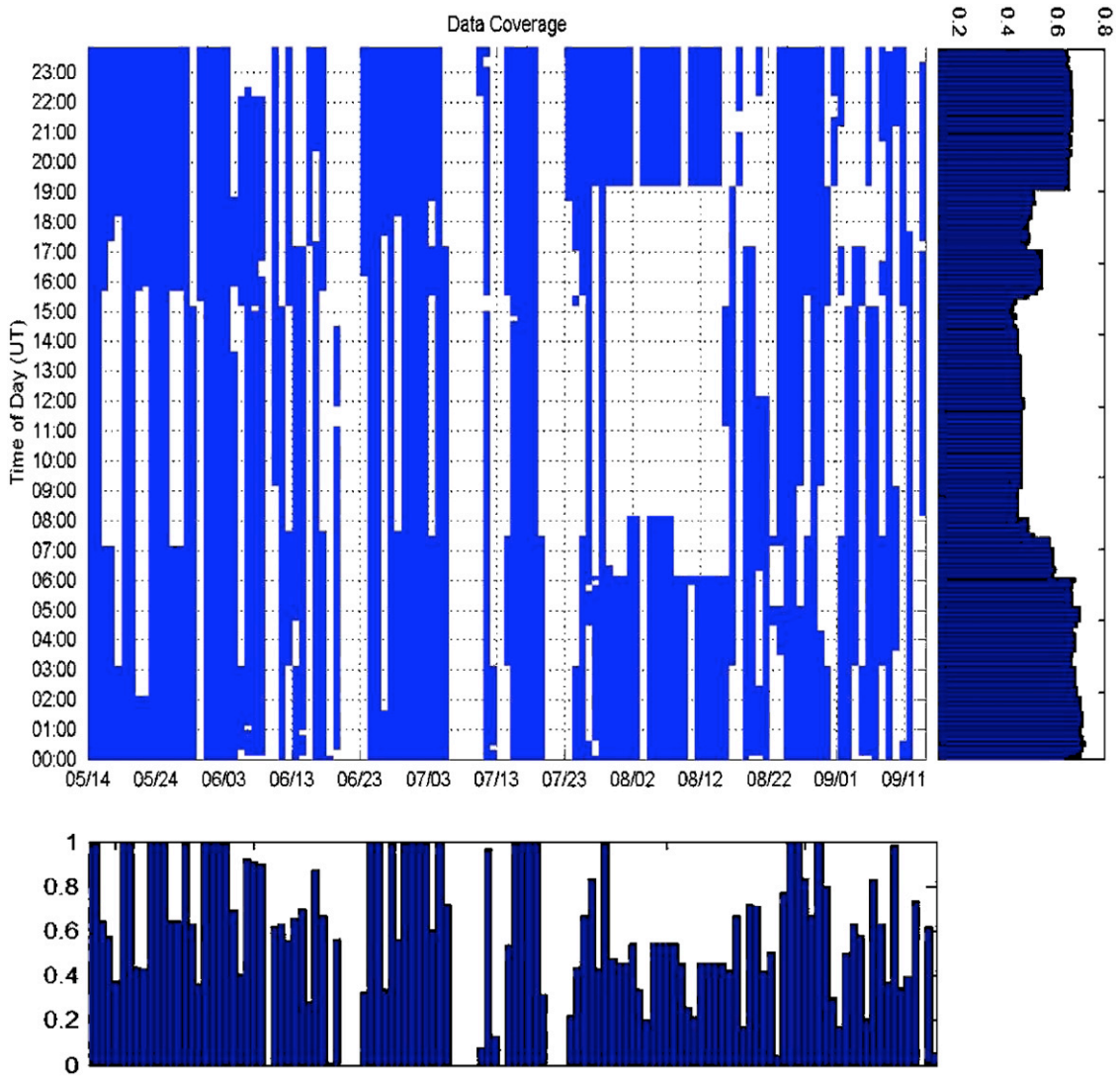

Fig. 1. Local time and date coverage of IPY-mode operations for the 4-month period from May 14 to September 14, 2007. The histograms below and to the right are the percentage of time the mode was operated during each day and time of day, respectively.

and early August. For the altitude gates centered at 76.8, 81.2, 85.5, and 89.9 km the reflectivities were computed for 4 min intervals. A three point running median was taken to eliminate strong short-lived echoes (e.g., meteors). If the reflectivity in the 81.2 km or 85.5 km gate was above $3 \times 10^{-18}\,\mathrm{m}^{-1}$ and was $3 \times 10^{-18}\,\mathrm{m}^{-1}$ higher than the reflectivity in both the 76.8 and 89.9 km gates then this was considered to be a PMSE. The second criterion ensures that the echoes are confined to narrow layers, which is a distinctive characteristic of PMSE. The background incoherent scatter in this region typically has a reflectivity less than $10^{-18}\,\mathrm{m}^{-1}$, except during aurora when it can exceed the PMSE threshold of $3 \times 10^{-18}\,\mathrm{m}^{-1}$. The aurora, however, will not be confined to a narrow layer like the PMSE, so the algorithm can distinguish PMSE from aurora. As described by Nicolls et al. (2007), the volume reflectivity is computed as $\eta = (P_r/P_t)(\sigma_e/\tau_p k_{sys})r^2$ where P_t and P_r are the transmitted and received power (calibrated as described earlier), $\sigma_e \approx 10^{-28}\,\mathrm{m}^2$ is the scattering cross section of a single electron, $\tau_p = 30\,\mu\mathrm{s}$ is the baud length, r is the range, and k_{sys} is a system constant. k_{sys} for this beam is roughly $10^{-19}\,\mathrm{m}^5/\mathrm{s}$, which was determined from daytime plasma line measurements, and is accurate to within ~20%. To accurately estimate the radar scattering cross section the first lag was used instead of the zeroth because the range resolution is better, and the decorrelation over a 30 μs interval will be negligible for the spectrally narrow PMSE. This calculation of reflectivity assumes that the PMSE is a volume scattering process that fills the beam, which given the relatively large size of each range gate and the patchy nature of PMSE structures is unlikely. Thus these reflectivities should be treated as lower bounds.

As an example, many PMSE events are visible in the plot of the reflectivity for 25 June 2007 shown in Fig. 2. The reflectivities in this plot are computed for 4 min intervals then put through a 3 point running median, which is exactly the same way the automated algorithm processes the data. Alaska Standard Time (AKST) is UTC-9, and the true solar local time at the longitude of PFISR is approximately 50 min behind AKST. This day had the most PMSE of any day in the study and was chosen as an example because it illustrates many different types of observations. The automated algorithm counted 12 different events during this day, nine of which were in the 81.2 km range gate. The strongest event occurs during the night, and is accompanied by auroral ionization. The other patchy echoes in the 81.2 and 85.5 km gates were also classified as PMSE because there is no other explanation for the presence of such thin layers at these altitudes.

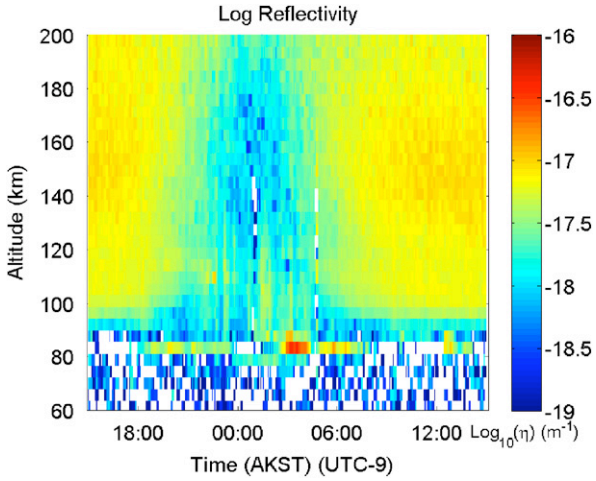

Fig. 2. Reflectivity for 6/25/07. Many PMSE are visible at 81 and 85 km. The strongest event is a nighttime PMSE accompanied by aurora.

Information about the spectral width of the PMSE can be obtained by fitting an exponential to the ACF measured at the altitude of the PMSE for the duration of the event. An exponential ACF corresponds to a Lorentzian power spectrum with a half-power half-width (HPHW) in rad/s equal to the e-folding time of the exponential. This HPHW can be expressed as a Doppler velocity by multiplying it by $\lambda_B/2\pi$ where $\lambda_B = 0.33$ m is the Bragg scattering wavelength of the radar. The event from 0235 to 0413 AKST on 25 June 2007 at 81.2 km was divided into periods of equal length which were approximately 8 min long, and the complex ACF was summed over each of these periods and adjusted to remove the triangular weighting. Fig. 3 is a plot of the magnitude of the sum of the complex ACFs for four of these 13 periods. The ACFs have been normalized such that the magnitude of the first lag is 1. As one might expect for PMSE, the ACFs are very nearly flat. The red curves are exponentials which have been fit to the magnitude of the ACF excluding the zeroth lag. The median of the HPHWs derived from these 13 fits is 2.0 ± 3.5 m/s. The error quoted is the standard deviation of the HPHWs measured from each 8 min period divided by the square root of the number of periods used. The zeroth lag was ignored when fitting the exponential because the information in the zeroth lag comes from a region smeared over the length of the pulse, of which only a thin band contains PMSE. The HPHW derived from these fits must be treated as a upper bound because these fits are extremely sensitive to small variations. The fits were done using a linear regression of the log of the magnitude of the ACF versus the lag, and the slope of this regression is the HPHW. The connection between short time periods and larger amounts of error in a measured slope can be illustrated by considering two points separated by a time difference t with values y_0 and $y_1 + \varepsilon$ where ε is the amount of error in y_1. The measured slope would be $m = (y_1 + \varepsilon - y_0)/t$. The error in the derived slope is ε/t, and is thus greatly magnified as t becomes short.

4. Discussion

Fig. 4 shows a histogram of the times of day for the PMSE in AKST. The times of day are the midpoint of the beginning and ending time of the event. The distribution peaks near solar noon, which is approximately 12:50 AKST. 2200 to 0400 LT corresponds roughly to the nighttime at this latitude and time of year.

The time of day dependence of PMSE might be more succinctly explained by a dependence on background ionization, and thus on solar zenith angle. Fig. 5 is a histogram of the solar zenith angles of the events. The times of the events were converted to solar zenith angles using the National Renewable Energy Laboratory, Measurement and Instrumentation Data Center, Solar Position Calculators (NREL, 2008). PMSE becomes more common as the zenith angle becomes lower. The large number of events at solar zenith angles near 90° are nighttime events. There were 48 events at solar zenith angles over 80° on 19 different nights. Thirty-one of these events, spanning 10 different nights, had auroral E-region ionization. PMSE at UHF accompanied by events which increase the background density has been observed before. Röttger et al. (1990) in Tromsø, Norway, and Cho et al. (1992b) in Sondrestrom, Greenland, which are two of the first observations of PMSE at UHF, both mention that their observations occurred during particle precipitation events which raised the D-region electron density. EISCAT observes PMSE accompanied by aurora at Tromsø but has not published these results (La Hoz, 2008, personal communication). At higher zenith angles the amount of local ionization may not be high enough to support PMSE at UHF. Necessary conditions for the occurrence of PMSE have been discussed by Rapp et al. (2002), and it is expected that there is a minimum threshold

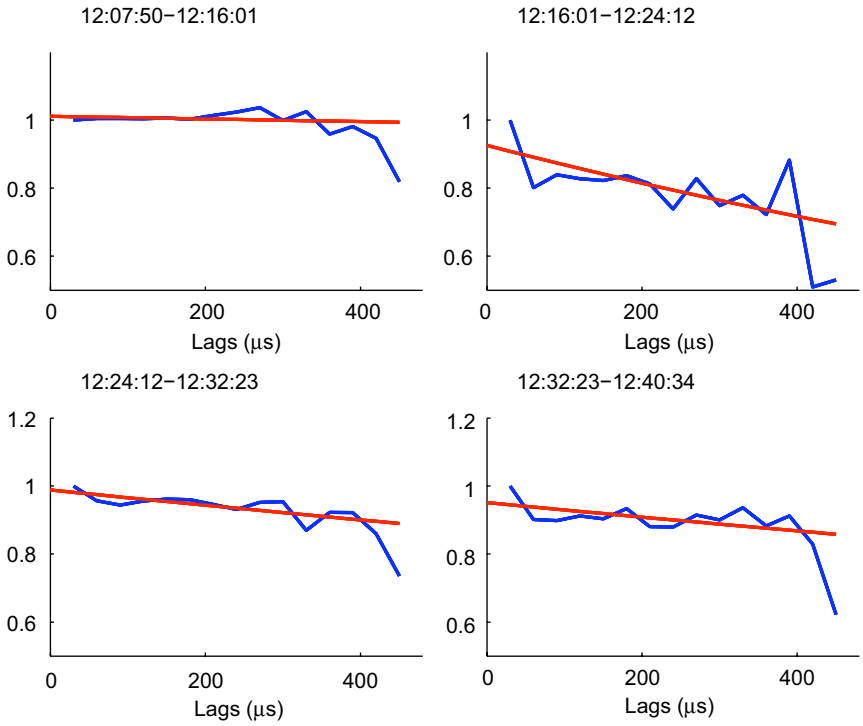

Fig. 3. Magnitudes of the summed ACF in arbitrary units for four time periods on 6/25/07 at 81.15 km. The data have been adjusted to remove the triangular weighting of the ACF. The red curves are exponential fits to the magnitude of the ACF, excluding the zeroth lag. The median of these fits was used to estimate the spectral width. (For interpretation of the references to color in this figure legend, the reader is referred to the web version of this article.)

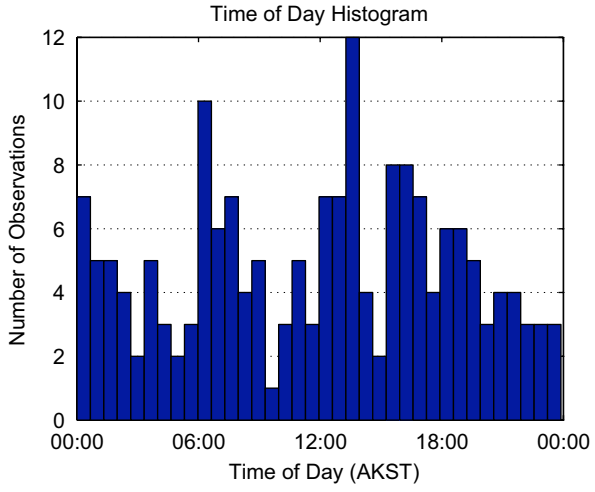

Fig. 4. Histogram of the times of day of the observed events. The distribution peaks near solar noon.

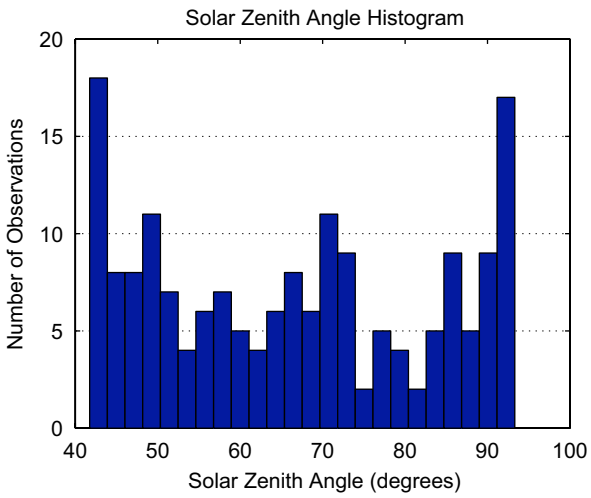

Fig. 5. Histogram of solar zenith angles. The rate of PMSE occurrence decreases as the zenith angle increases. However, there are also many events during the night which are associated with aurora.

density of $\sim 10^9\,\mathrm{m}^{-3}$ where PMSE can occur. This can be understood by the fact that the radar scattering cross section is proportional to the power spectral density of the electron density fluctuations, the upper limit of which is dictated by the density itself. For low densities, the electron density should be correlated with PMSE reflectivity. At very high densities, however, PMSE seems to be not at all or negatively correlated with the absolute density. Rapp et al. (2002) have explained this based on the fact that above a certain point the fraction of charge bound to the aerosol particles (the so-called Havnes parameter) will decrease due to saturation (e.g., Rapp and Lübken, 2001). Above this level, an increase in density will lead to an increase in electron diffusion, causing a negative correlation with density until the PMSE ultimately disappears.

Fig. 6 shows the distribution of PMSE for different days of the year. Each bin in the bar graph ranges from 0 to 0 UT the following day. For each bin the duration of all the PMSE events in the bin was summed. When PMSE was observed simultaneously in both the 81.2 and 85.5 km altitude gates the duration of the overlap was not double counted. Thus the graph shows the number of hours of PMSE per day. IPY data were examined beginning in March 2007, but the first PMSE event was not observed until May 27. Data were also examined until September 14, but no PMSE was observed after August 10. PMSE appear to be most common in the middle of this period, in late June and early July, with some days having many hours of PMSE. The day with the most PMSE is June 25, the day used as an example above, with

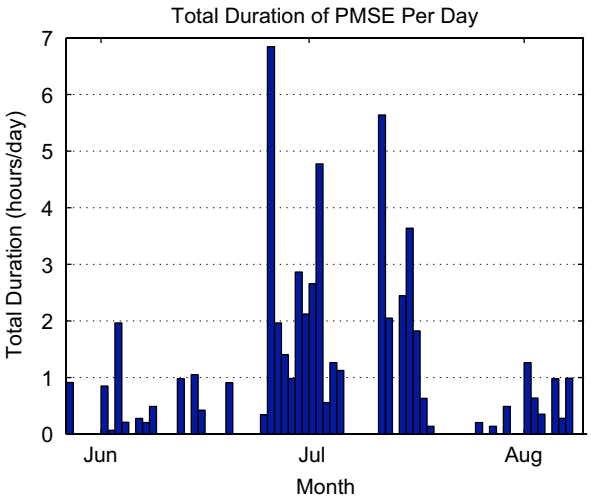

Fig. 6. Average total duration of all PMSE events per day. PMSE events start to appear in late May and stop appearing after mid-August. Late June and July have the most PMSE.

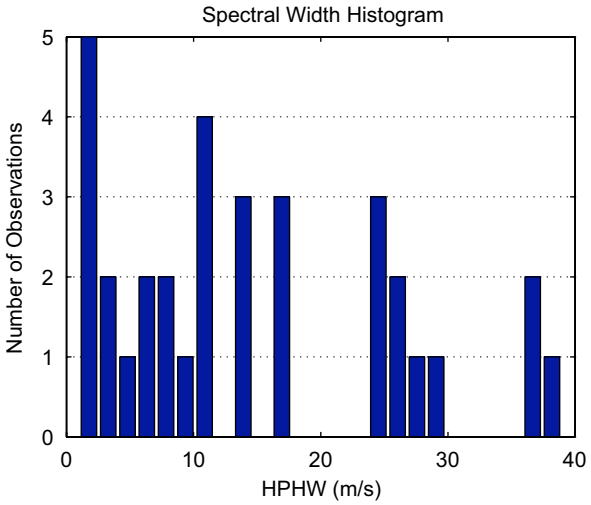

Fig. 7. Histogram of HPHW. The mean HPHW is 14.8 m/s, with a deviation of 11.1 m/s.

over 6 h of PMSE. These results are similar to the statistical study with a 50 MHz MST radar at the same site by Ecklund and Balsley (1981) and Balsley et al. (1983).

A histogram of the measured HPHWs is shown in Fig. 7. The HPHWs were computed as in the example above, by dividing the event into periods of approximately 8 min, fitting an exponential to the magnitude of the summed complex ACF over each period, and then taking a median. If the Doppler shift is changing significantly during these 8 min periods then summing the complex ACF will underestimate the mean magnitude of the ACF, resulting in an overestimate of the spectral width. Thus these measurements should be treated as upper bounds. The HPHWs for the 111 events with reflectivities below $8.0 \times 10^{-18}\,\mathrm{m}^{-1}$ are not included because the measurement of the HPHW is highly inaccurate for weak signals. During weak events the PMSE is almost certainly not filling the beam, meaning the spectrum will be a combination of the PMSE spectrum and the background ISR spectrum. This makes a measurement of the PMSE spectrum difficult. Of the strong events, 26 more events were omitted because the HPHWs were too small to measure. The slope of the ACF was so low that most of the regressions resulted in a positive slope due to small fluctuations, which is not physical. Of the events with measurable HPHWs, the mean was 14.8 m/s with a standard deviation of 11.1 m/s, excluding six events with widths over 50 m/s. The large amount of error in this estimation of the spectral width is due to the use of a 480 μs ACF to measure a decorrelation time which is several milliseconds long. La Hoz et al. (2006) measured spectral widths for PMSE between 1.8 and 12 m/s with the EISCAT 933 MHz. Their widths are the standard deviation of a Gaussian distribution function. These can be converted to HPHWs by multiplying by $\sqrt{2\ln 2}$, resulting in HPHWs ranging from 2.1 to 14 m/s. Our HPHWs agree with their upper bound of 14 m/s, and we do not have the spectral resolution to reproduce their lower bound. Nicolls et al. (2008), based on one night of observations, showed a similar range of spectral widths, with most echoes being quite narrow (1–2 m/s).

Fig. 8 is a histogram summarizing the durations of the PMSE events. The mean duration is 19.6 min, and the median is 12.5 min. Short durations are the most common, but two exceptional events with durations of 97.9 and 106.4 min were observed. If PFISR operated at 50 MHz these durations would be consistent with the estimates of Rapp and Lübken (2003) for the duration of 3-m (50 MHz) echoes after a given "pulse" of neutral turbulence. These estimates indicate that PMSE should last tens of minutes after turbulence turn-off due to the slower electron diffusion rate (thus not requiring the existence of neutral air turbulence within the scattering volume). However, at 450 MHz, the diffusion times are approximately two orders of magnitude shorter (going as the square of the wavelength) than those estimates. This seems to imply that a persistent turbulence generation mechanism is necessary, indicating that PMSE at these frequencies should be tightly coupled to the presence of active neutral air turbulence. However, as evidenced by the observations of Nicolls et al. (2008), most echoes are fairly long-lived and spectrally narrow, implying that they have evolved from a turbulent source and become fossilized within the background plasma, allowing them to drift through the field of view with the background winds. At this point, the expected lifetime of these fossilized echoes based on turbulence theory is somewhat unclear and will depend at least in part on the background ionospheric conditions.

The measured reflectivities of the events are summarized in Fig. 9. Each 4 min period used by the automated algorithm is used in this histogram instead of using one point per event because PMSE events are not expected to have a constant reflectivity. The highest reflectivity observed was $3.6 \times 10^{-16}\,\mathrm{m}^{-1}$. The reflectivities had a mean of $1.3 \times 10^{-17}\,\mathrm{m}^{-1}$ with a standard deviation of

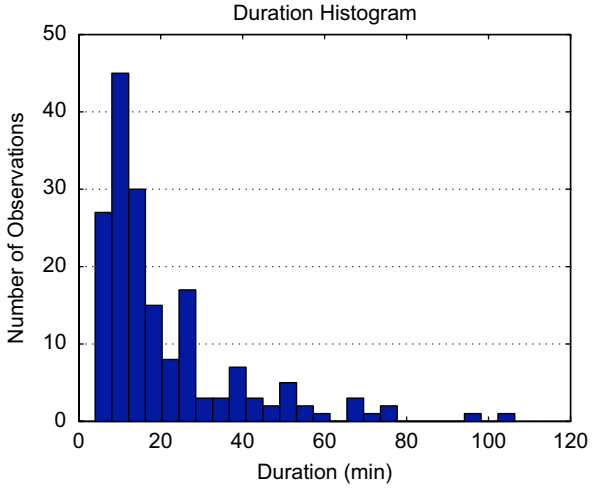

Fig. 8. Histogram of the PMSE durations, in minutes. The mean duration is 19.6 min with small durations being the most common.

$3.1 \times 10^{-17}\,\mathrm{m}^{-1}$. These estimates underestimate the true reflectivity because we have assumed the beam is filled with volume scattering structures.

To give some basis for comparison we list PMSE reflectivities measured at different sites and frequencies in Table 1. These results were compiled by Rapp and Lübken (2004). These reflectivities along with our average and maximum observed reflectivity are plotted versus their radar Bragg wavenumbers in Fig. 10. The radar Bragg wavenumber is here defined as $k = 2\pi/\lambda_B$ where λ_B is the Bragg scattering wavelength of the radar. We have also plotted a model for the reflectivity for three different Schmidt numbers. The model used is described by Rapp et al. (2008). We have assumed typical values of $0.5\,\mathrm{m}^2/\mathrm{s}$ for the viscosity, 4 km for the scale height, and 5 min for the Brunt Väisälä period. We have assumed moderate values of 0.05 W/kg for the energy dissipation rate, $5 \times 10^9\,\mathrm{m}^{-3}$ for the electron density, and $1.5 \times 10^6\,\mathrm{m}^{-4}$ for the vertical electron density gradient. Under these assumptions all of our reflectivities can be explained by a Schmidt number of $\sim$200–500. However, as discussed earlier we are almost certainly underestimating the reflectivity, so these estimates of the Schmidt number are also too low. Recent work by Rapp et al. (2008) suggests that the Schmidt numbers associated with PMSE are actually several 1000s.

Finally, Fig. 11 is a scatter plot of the spectral width versus the reflectivity. All events which were excluded from the histogram in Fig. 7 have also been excluded here. No correlation between signal strength and spectral width was observed. This result is consistent with isotropic scatter at this frequency, which was suggested by Nicolls et al. (2007) using the fact that PFISR observes roughly constant volume scattering cross sections for a range of off-zenith angles. These observations are in contrast to those at VHF, where a correlation between signal strength and spectral width is observed (along with aspect sensitive scatter) (e.g., Cho and Röttger, 1997; Chilson et al., 2002; Rapp and Lübken, 2004), but are perhaps consistent with active turbulence within the scattering volume.

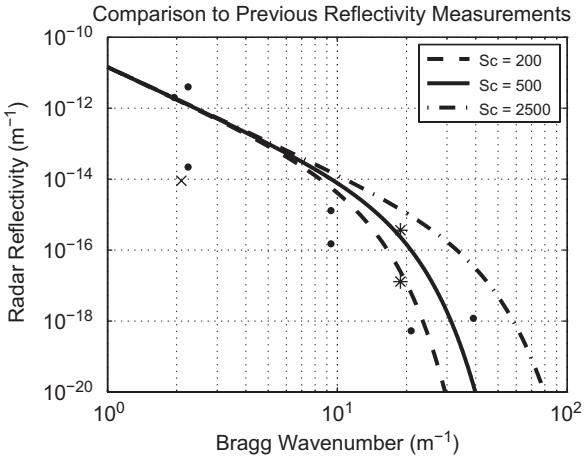

Fig. 10. Plot of reflectivity versus radar Bragg wavenumber. The $*$ denote our mean and maximum observed reflectivity. The rest of the points are taken from Table 1. The $\times$ is the other measurement made at Poker Flat. Curves for three different Schmidt numbers assuming typical values for the other parameters are also shown.

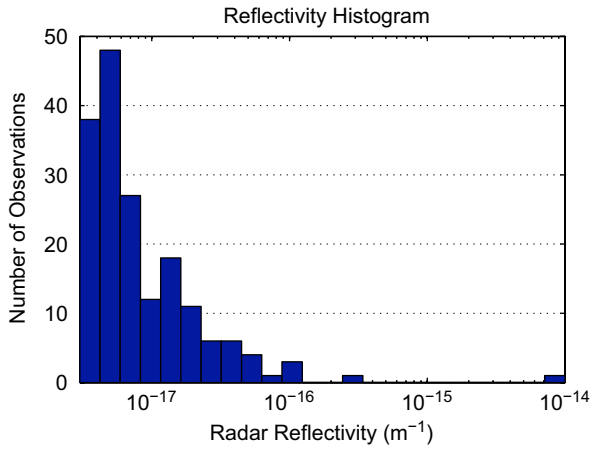

Fig. 9. Histogram of signal strength, expressed in reflectivity in m^{-1}. The mean strength is $1.3 \times 10^{-17}\,\mathrm{m}^{-1}$.

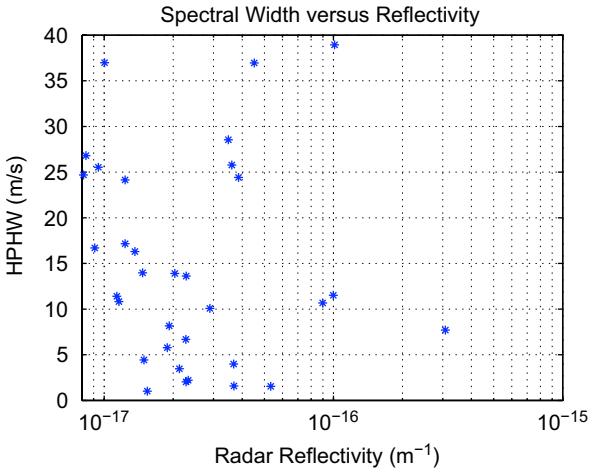

Fig. 11. Scatter plot of spectral width versus reflectivity. No correlation between the two parameters was observed.

Table 1
Previous measurements of PMSE reflectivity.

Frequency (Bragg scale) (MHz (m))	Location	Reference	Reflectivity (m^{-1})
49.6 (3.0)	Tromsø (69°N)	Röttger et al. (1990)	2.0×10^{-12}
50.0 (3.0)	Poker Flat (65°N)	Kelley and Ulwick (1988)	9.0×10^{-15}
53.5 (2.8)	Andøya (69°N)	Inhester et al. (1990)	4.0×10^{-12}
53.5 (2.8)	Svalbard (78°N)	Röttger (2001)	2.2×10^{-14}
224 (0.67)	Tromsø (69°N)	Hoppe et al. (1988)	1.5×10^{-16}
500 (0.3)	Svalbard (78°N)	Röttger (2001)	5.3×10^{-19}
933 (0.16)	Tromsø (69°N)	Röttger et al. (1990)	1.2×10^{-18}

5. Summary and conclusions

We have found 176 examples of PMSE recorded by PFISR in the IPY mode during the summer of 2007. PMSE were observed 3.35% of the time during the period from May 14 until September 14, with the first and last observations being on May 27 and August 10. Seventy-three percent of the events were observed during the daytime, and 38% of the days had at least one event. PMSE were also observed at night, and most of these nighttime events was accompanied by aurora. This, combined with the strong preference for higher solar zenith angle for daytime PMSE, suggests that PMSE is strongly dependent on the level of background ionization (e.g., Rapp et al., 2002). The events all occurred in either the 81.15 or 85.54 km altitude bins. The PMSE have a mean duration of 19.6 min, which is much longer than the electron diffusion time scale at this Bragg wavelength (e.g., Rapp and Lübken, 2003). The mean reflectivity of the observations was $\sim 1.3 \times 10^{-17}\,\mathrm{m}^{-1}$. A Lorentzian power spectrum was assumed, and the HPHW was measured by fitting an exponential to the measured ACFs. The mean of the measurable HPHWs was $14.8 \pm 11.1\,\mathrm{m/s}$. The large amount of error in this measurement is primarily due to the use of a 480 μs pulse to measure a plasma ACF with much longer correlation times. Thus, this estimate is most certainly an upper bound, as indicated by the error estimates.

Acknowledgments

The PFISR was developed under NSF cooperative agreement ATM-0121483, and the data collection and analysis was supported under NSF cooperative agreement ATM-0608577. Work at Cornell was sponsored by the Atmospheric Science Division of the National Science Foundation under Grant ATM-0538343.

References

Balsley, B.B., Ecklund, W.L., Fritts, D.C., 1983. Mesospheric radar echoes at Poker Flat, Alaska: evidence for seasonally dependent generation mechanisms. Radio Sci. 18, 1053–1058.

Chilson, P.B., Yu, T.-Y., Palmer, R.D., Kirkwood, S., 2002. Aspect sensitivity measurements of polar mesosphere summer echoes using coherent radar imaging. Ann. Geophys. 20, 213–223.

Cho, J.Y.N., Röttger, J., 1997. An updated review of polar mesosphere summer echoes: observation, theory, and their relationship to noctilucent clouds and subvisible aerosols. J. Geophys. Res. 102, 2001–2020.

Cho, J.Y.N., Hall, T.M., Kelley, M.C., 1992a. On the role of charged aerosols in polar mesosphere summer echoes. J. Geophys. Res. 97, 875–886.

Cho, J.Y.N., Kelley, M.C., Heinselman, C.J., 1992b. Enhancement of Thomson scatter by charged aerosols in the polar mesosphere: measurements with a 1.29 GHz radar. Geophys. Res. Lett. 19, 1097–1100.

Czechowsky, P., Rüster, R., Schmidt, G., 1979. Variations of mesospheric structures in different seasons. Geophys. Res. Lett. 6, 459–462.

Ecklund, W.L., Balsley, B.B., 1981. Long term observations of the arctic mesosphere with the MST radar at Poker Flat, Alaska. J. Geophys. Res. 86, 7775–7780.

Fritts, D.C., Bizon, C., Werne, J.A., Meyer, C.K., 2003. Layering accompanying turbulence generation due to shear instability and gravity-wave braking. J. Geophys. Res. 108.

Gibson-Wilde, D., Werne, J., Fritts, D., Hill, R., 2000. Direct numerical simulation of VHF radar measurements of turbulence in the mesosphere. Radio Sci. 35, 783–798.

Hall, C.M., Röttger, J., 2001. Initial observations of polar mesospheric summer echoes using the EISCAT Svalbard Radar. Geophys. Res. Lett. 28, 131–134.

Hoppe, U.-P., Hall, C., Röttger, J., 1988. First observations of summer polar mesospheric backscatter with a 224 MHz radar. Geophys. Res. Lett. 15, 28–31.

Inhester, B., Ulwick, J., Cho, J., Kelley, M., Schmidt, G., 1990. Consistency of rocket and radar electron density observations: implications about the anisotropy of turbulence. J. Atmos. Terr. Phys. 52, 855–873.

Kelley, M.C., Ulwick, J.C., 1988. Large and small-scale organization of electrons in the high-latitude mesosphere: implications of the STATE data. J. Geophys. Res. 93, 7001–7008.

Kelley, M.C., Farley, D.T., Röttger, J., 1987. The effect of cluster ions on anomalous VHF backscatter from the summer polar mesosphere. Geophys. Res. Lett. 14, 1031–1034.

La Hoz, C., 2008. Personal communication.

La Hoz, C., Havnes, O., Naesheim, L.I., Hysell, D.L., 2006. Observations and theories of polar mesospheric summer echoes at a Bragg wavelength of 16 cm. J. Geophys. Res. 111.

Lehtinen, M.S., Häggström, I., 1987. A new modulation principle for incoherent scatter measurements. Radio Sci. 22, 625–634.

Lübken, F.-J., Rapp, M., Hoffmann, P., 2002. Neutral air turbulence and temperatures in the vicinity of polar mesosphere summer echoes. J. Geophys. Res. 107.

Nicolls, M., Kelley, M., Varney, R., Heinselman, C., 2008. Spectral observations of polar mesospheric summer echoes at 33 cm (450 MHz) with the Poker Flat Incoherent Scatter Radar. J. Atmos. Solar-Terr. Phys., in press, doi:10.1016/j.jastp.2008.04.019.

Nicolls, M.J., Heinselman, C.J., Hope, E.A., Ranjan, S., Kelley, M.C., Kelly, J.D., 2007. Imaging of polar mesosphere summer echoes with the 450 MHz Poker Flat Advanced Modular Incoherent Scatter Radar. Geophys. Res. Lett. 34.

NREL, National renewable energy laboratory, measurement and instrumentation data center, solar position calculators. ⟨http://www.nrel.gov/midc/solpos/solpos.html⟩.

Rapp, M., Lübken, F.-J., 2001. Modelling of particle charging in the polar summer mesosphere: 1. General results. J. Atmos. Solar-Terr. Phys. 63, 759–770.

Rapp, M., Lübken, F.-J., 2003. On the nature of PMSE: electron diffusion in the vicinity of charged particles revisited. J. Geophys. Res. 108.

Rapp, M., Lübken, F.-J., 2004. Polar mesosphere summer echoes (PMSE): review of observations and current understanding. Atmos. Chem. Phys. 4, 2601–2633.

Rapp, M., Gumbel, J., Lübken, F.-J., Latteck, R., 2002. *D* region electron number density limits for the existence of polar mesosphere summer echoes. J. Geophys. Res. 107.

Rapp, M., Strelnikova, I., Latteck, R., Hoffman, P., Hoppe, U.-P., Häggström, I., Rietveld, M., 2008. Polar mesosphere summer echoes (PMSE) studied at Bragg wavelengths of 2.8 m 67 cm and 16 cm. J. Atmos. Solar-Terr. Phys. 70, 947–961.

Röttger, J., 2001. Observations of the polar D-region and the mesosphere with the EISCAT Svalbard Radar and the SOUSY Svalbard Radar. Mem. Nat. Inst. Pol. Res. 54, 9–20.

Röttger, J., Hoz, C.L., Kelley, M.C., Hoppe, U.P., Hall, C., 1988. The structure and dynamics of polar mesosphere summer echoes observed with the EISCAT 224 MHz radar. Geophys. Res. Lett. 15, 1353–1356.

Röttger, J., Rietveld, M.T., La Hoz, C., Hall, C., Kelley, M.C., Swartz, W.E., 1990. Polar mesosphere summer echoes observed with the EISCAT 933-MHz radar and the CUPRI 469-MHz radar, their similarity to 224-MHz radar, echoes, and their relation to turbulence and electron density profiles. Radio Sci. 25, 671–687.